Coupled Analysis of Change in Fracture Permeability during the Cooling Phase of the Yucca Mountain Drift Scale Test

Rutqvist, J., Freifeld, B. and Tsang, Y.W.
Earth Sciences Division, Lawrence Berkeley National Laboratory, Berkeley, CA 94720, USA
Min, K.B. and Elsworth, D.
Department of Energy and Geo-Environmental Eng., Pennsylvania State University, University Park, PA 16802, USA

ABSTRACT: This paper presents results from a coupled thermal, hydrological and mechanical analysis of thermally-induced permeability changes during heating and cooling of fractured volcanic rock at the Drift Scale Test at Yucca Mountain, Nevada. The analysis extends the previous analysis of the four-year heating phase to include newly available data from the subsequent four-year cooling phase. The new analysis of the cooling phase shows that the measured changes in fracture permeability follows that of a thermo-hydro-elastic model on average, but at several locations the measured permeability indicates (inelastic) irreversible behavior. At the end of the cooling phase, the air-permeability had decreased at some locations (to as low as 0.2 of initial), whereas it had increased at other locations (to as high as 1.8 of initial). Our analysis shows that such irreversible changes in fracture permeability are consistent with either inelastic fracture shear dilation (where permeability increased) or inelastic fracture surface asperity shortening (where permeability decreased). These data are important for bounding model predictions of potential thermally-induced changes in rock-mass permeability at a future repository at Yucca Mountain.

1. INTRODUCTION

The Yucca Mountain Drift Scale Test (DST) is a multiyear, large-scale, underground heating test conducted by the U.S. Department of Energy in unsaturated fractured volcanic tuff at Yucca Mountain, Nevada (Fig. 1a) [1]. The DST, which started in 1997, included a four-year period of forced heating, followed by a four-year period of unforced (natural) cooling (Fig. 1b). Heating was provided by nine floor heaters within the heated drift, as well as 50 rod heaters, referred to as "wing heaters," placed into horizontal boreholes emanating from the heated drift. During the experiment, a volume of over 100,000 m^3 of intensively fractured volcanic tuff was heated, including several-tens-of-thousands of cubic meters heated to above boiling temperature (Fig. 1a). This massive heating induced strongly coupled thermal-hydrological-mechanical-chemical (THMC) changes that were continuously monitored by thousands of sensors embedded in the fractured rock mass. Of particular interest to this study is the periodic active pneumatic (air-injection) testing used to track changes in air permeability within the variably saturated fracture system around the DST. Air-injection testing was conducted in several-meters-long packed-off sections in 44 hydrological boreholes, in 3 clusters forming vertical fans that bracket the heated drift and the wing heaters (Fig. 2). In total, about 700 air-injection tests were performed in the 44 packed-off sections during the course of the four-year heating and four-year cooling periods.

Previous coupled thermal-hydrological-mechanical (THM) analyses of the initial four-year heating period (lasting from December 1997 through January 2002) indicated that the observed air-permeability changes were a result of both thermal-mechanical (TM) changes in fracture aperture and thermal-hydrological (TH) changes in fracture moisture content [2, 3, 4]. Moreover, those previous analyses indicated that the TM-induced changes in fracture aperture and intrinsic permeability would be mostly reversible. However, the prediction of reversible behavior was based on analysis of data from the four-year heating period and did not include the data from the subsequent four-year cooling period.

In this paper, we present results from an extension of our THM analysis to include thermally induced permeability changes measured during the four-year cooling period, from January 2002 through November 2005. Studying the cooling phase provides an opportunity to investigate whether the observed permeability changes are permanent (irreversible), in which case they would persist after the temperature has cooled down to ambient.

For this new analysis of the cooling phase, we employed the same model setup as in the previous analysis of the heating phase [2]. That is, we simulated the DST in a

two-dimensional vertical cross section oriented perpendicular to the tunnel axis (Fig. 3a). To achieve an accurate representation of the temperature evolution during the cooling phase, we had to consider two- to three-dimensional out-of-plane heat loss in the rock mass as well as heat loss through the bulk head at entrance of the heated drift. Using such an approach, we achieved a very good agreement between calculated and measured temperature, as shown in Fig. 1b. Moreover, we conducted a new model calibration of a stress-versus-permeability function for the fractured rock, considering data from all the 700 air-injection tests. The field data from all these tests in the 44 borehole intervals, as well as the calibration of the stress-versus-permeability function, are presented in detail in Rutqvist et al. [5]. In this paper we briefly present the model and then focus on results at a few measurement locations that indicate either elastic (reversible) or inelastic (irreversible) mechanical changes at the end of the cooling period.

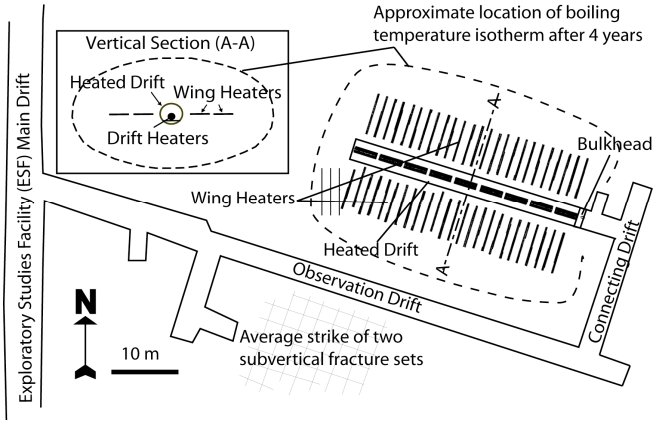

(a)

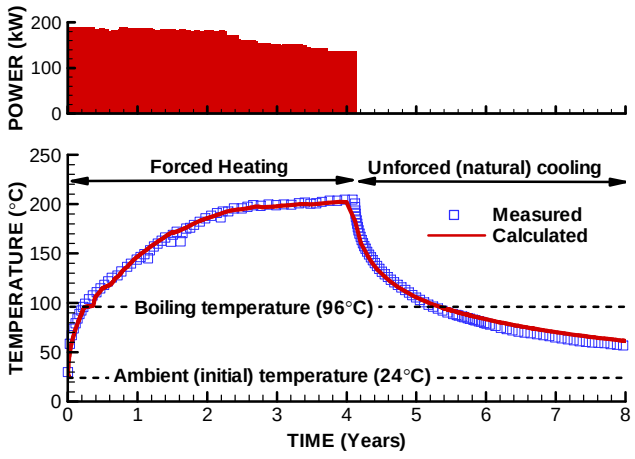

(b)

Fig. 1. The Yucca Mountain Drift Scale Test: (a) Layout and approximate measured extent of the boiling isotherm (96°C) after four years of heating; (b) Evolution of heat power (total power in drift and wing heaters) and measured drift-wall temperature at a point located at the top of the drift about 10 cm into the rock.

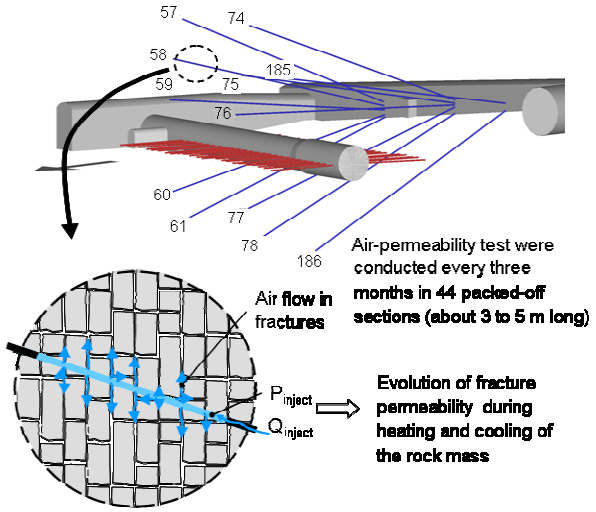

Fig. 2. Three-dimensional view of DST and boreholes for air-permeability testing, and a close-up illustration of air-injection testing in one borehole interval.

2. MODEL SETUP

The model conceptualization is equivalent to that used for modeling of the heating phase [2]. The DST is simulated with TOUGH-FLAC, a simulator for modeling multiphase fluid and heat transport, coupled with geomechanical stress and strain analysis [6]. The two-dimensional cross section is 250 m high and 200 m wide. The highly fractured rock mass at the test site was modeled as a dual-permeability medium, which consists of interacting matrix and fracture continua (Fig. 3a) [7, 8].

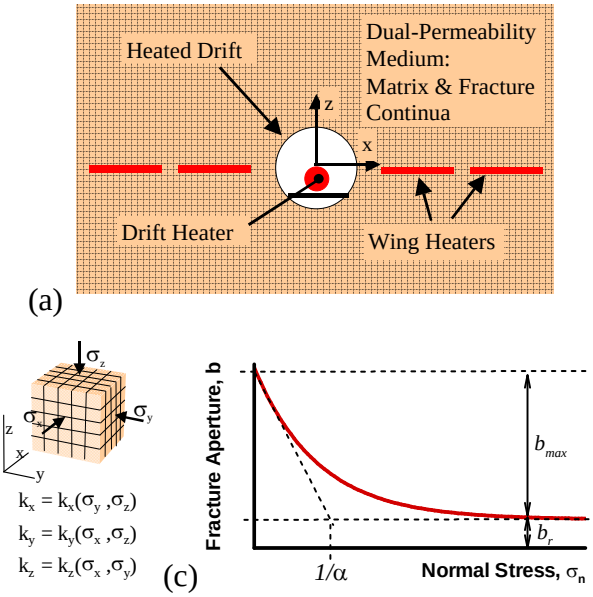

Fig. 3. TOUGH-FLAC simulation model of the DST: (a) schematics of two-dimensional model geometry and dual-permeability model; (b) conceptual model for stress-permeability coupling; (c) normal stress versus aperture relationship for fractures.

The dual-permeability continuum model approach has been proven suitable for modeling of fluid flow and heat transfer in the unsaturated zone at Yucca Mountain, since it realistically captures the partitioning of simultaneous fluid flow in both the fractures and rock matrix. The continuum approach is deemed appropriate, because the rock mass in the unsaturated zone at Yucca Mountain is intensively fractured. Fracture mapping at the site shows three dominating fracture sets [9]:

(i) prominent vertical, southeast trending

(ii) vertical, southwest trending

(iii) subhorizontal.

The average spacing for mapped fractures of length larger than 1 m is about 0.3 to 0.4 m. However, detailed cell mapping has shown that about 80% of the fractures at the site are less than one meter; thus, the fracture spacing counting all fractures would be less than 0.3 m. Moreover, air-permeability tests conducted in short-interval (0.3 m) packed-off borehole sections show that vertical fluid conducting fractures exist at least every 0.3 m [10]. This evidence of a highly fractured rock justifies the use of a continuum modeling approach.

An important part of this analysis is the coupled hydromechanical model of the fractured rock. In this study, we employ a hydromechanical model that considers changes in porosity, permeability, and capillarity in the fractured continua as a result of stress-induced changes in fracture apertures. Changes in hydrological properties are calculated using a conceptual model of three orthogonal fracture sets consistent with the three main fracture sets observed at the site (Fig. 3b). Using this conceptual model, the porosity, permeability, and capillary pressure in the fracture continuum are corrected for any change in the stress field, according to:

$$\phi = F_{\phi} \times \phi_i \tag{1}$$

$$k_x = F_{kx} \times k_{ix},\ k_y = F_{ky} \times k_{iy},\ k_z = F_{kz} \times k_{iz} \tag{2}$$

$$P_c = F_{Pc} \times P_{ci} \tag{3}$$

where F denotes various correction factors, subscripts ϕ, k and c refers to correction factors for porosity, permeability and capillarity, respectively, and subscript i denotes initial (preheating) conditions. Note that although the simulation is conducted in a two-dimensional plane strain model, stress in the out-of-plane direction (y direction) is calculated, and changes in the three-dimensional permeability field can therefore be evaluated. The permeability along x, y, and z directions are calculated from the aperture, b, and spacing, s, of fractures belonging to fracture sets 1, 2, and 3, using a parallel-plate fracture flow model [11] according to:

$$k_x = \frac{b_2^3}{12 s_2} + \frac{b_3^3}{12 s_3} \tag{4a}$$

$$k_y = \frac{b_1^3}{12 s_1} + \frac{b_3^3}{12 s_3} \tag{4b}$$

$$k_z = \frac{b_1^3}{12 s_1} + \frac{b_2^3}{12 s_2} \tag{4c}$$

where subscripts 1, 2, and 3 denotes the three orthogonal fracture sets, assumed to be oriented normal to x, y, and z directions, respectively. Porosity and permeability correction factors are calculated from the initial and current apertures, b, according to:

$$F_{\phi} = \frac{b_1/s_1 + b_2/s_2 + b_3/s_3}{b_{1i}/s_1 + b_{2i}/s_2 + b_{3i}/s_3} \tag{5}$$

$$F_{kx} = \frac{b_2^3/s_2 + b_3^3/s_3}{b_{2i}^3/s_2 + b_{3i}^3/s_3} \tag{6a}$$

$$F_{ky} = \frac{b_1^3/s_1 + b_3^3/s_3}{b_{1i}^3/s_1 + b_{3i}^3/s_3} \tag{6b}$$

$$F_{kz} = \frac{b_1^3/s_1 + b_2^3/s_2}{b_{1i}^3/s_1 + b_{2i}^3/s_2} \tag{6c}$$

A simplified version of these correction factors can be derived by assuming equal spacing in the three orthogonal fracture sets, leading to:

$$F_{\phi} = \frac{b_1 + b_2 + b_3}{b_{1i} + b_{2i} + b_{3i}} \tag{7}$$

$$F_{kx} = \frac{b_2^3 + b_3^3}{b_{2i}^3 + b_{3i}^3} \tag{8a}$$

$$F_{ky} = \frac{b_1^3 + b_3^3}{b_{1i}^3 + b_{3i}^3} \tag{8b}$$

$$F_{kz} = \frac{b_1^3 + b_2^3}{b_{1i}^3 + b_{2i}^3} \tag{8c}$$

In this study, we used Equation (7) and (8), which are consistent with both the model used for the analysis of the heating period and the isotropic hydrological models of the site [2, 8]. Moreover, using the above equations is justified, considering that unequal fracture spacing for the different fracture sets would have a very small impact on the calculated stress-induced changes in permeability—because such changes are dominated by the cubic dependency on aperture.

The capillary pressure is corrected with porosity and permeability changes according to the Leverett [12] function:

$$F_{Pc} = \sqrt{\frac{F_\phi}{F_k}} \quad (9)$$

where

$$F_k = \sqrt[3]{F_{kx} \times F_{ky} \times F_{kz}} \quad (10)$$

Thus, in areas where permeability increases as the fractures opens, the capillarity tends to decrease.

The current fracture aperture b depends on the current effective normal stress σ'_n, according to the following exponential function [6]:

$$b = b_r + b_m = b_r + b_{\max}\left[\exp(\alpha\sigma_n)\right] \quad (11)$$

where b_r is a residual aperture, b_m is a mechanical aperture, b_{max} is the mechanical aperture corresponding to zero normal stress, and α is a parameter related to the curvature of the function (Fig. 3c). This relationship can also be expressed in terms of an initial aperture, b_i, and changes in aperture, Δb, as:

$$b = b_i + \Delta b = b_i + b_{\max}\left[\exp(\alpha\sigma_n) - \exp(\alpha\sigma_{ni})\right] \quad (12)$$

where σ_{ni} is the initial stress normal to the fractures. In Equations (11) and (12), the engineering sign convention is used for effective normal stress, which implies that tensile stress is positive and compressive stress is negative. These expressions can be inserted into Equation (8) to derive expressions for rock-mass permeability correction factors in x, y, and z directions.

3. MATERIAL PROPERTIES AND INITIAL CONDITIONS

The basic material properties of the rock mass surrounding the DST are presented in Table 1. These include both matrix and fracture hydrological properties for the dual-continuum approach as well as equivalent continuum rock-mass mechanical properties. Hydrological properties include water-retention curves and relative permeability functions based on van-Genuchten's [13] model. Mechanical properties include a fractured rock-mass deformation modulus of 14.77 GPa, which is about 50% lower than the Young's modulus of intact rock. A temperature-dependent thermal expansion coefficient is adopted [2].

The parameters b_{max}, α and b_r defining the stress-aperture relationship in Equations (11) and (12) were determined by model calibration. The investigation and calibration of the stress-aperture relationship is described in Rutqvist et al. [5], and involves detailed interpretation of the above mentioned air-injection tests. The model calibration was conducted in steps: first we made an accurate model simulation of the temperature field, which is the basic driving force behind both the moisture induced-changes in relative permeability and stress-induced changes in fracture aperture. After confirming a good agreement between the measured and calculated temperature field, we calculated and sampled the evolution of stress and gas saturation at each air-injection interval in order to calculate the air-permeability evolution, which in turn could be directly compared to the measured air-permeability evolution.

The basic parameters b_{max}, α and b_r in Eq. (11) or b_{max}, α and b_i in Eq. (12) were calibrated to achieve the best match of the average evolution in permeability for all 44 packed-off intervals. Following the calibration method described in Rutqvist et al. [5], we need only to calibrate two of the three parameters (e.g. b_{max} and α) because b_i can be determined directly from the measured initial permeability. The calibration was conducted assuming that the measured permeability changes were caused by changes in the major NW-striking subvertical fracture set. Fractures in this fracture set strike approximately perpendicular to the subhorizontal monitoring boreholes, which implies that they are most likely to be hydraulically connected to the boreholes (see illustration Fig. 2).

The final calibrated parameters valid for the applied conceptual stress-versus-permeability model, with initial permeability of 1×10^{-13} m^2 and fracture spacing of 0.23 m, are b_{max} = 37.6 μm, α = 0.07 MPa^{-1} and b_r = 22.1 μm. These are the basic calibrated stress-aperture parameters applied when deriving model results presented in this paper.

Initial conditions are presented in Table 2. The initial stress, temperature, and phase saturations shown in Table 2 are the results of an initial steady-state simulation with fixed temperature conditions on the top and bottom of the model, and vertical water infiltration of 6 mm/year at the top of the model. At Yucca Mountain, vertical stress resulting from the weight of the overlying rock is the maximum principal stress, whereas the two horizontal principal stresses are estimated to be about half the magnitude of the vertical stress. At ambient (initial) conditions, the matrix is almost fully saturated with water, whereas fractures are likely almost dry (as a result of matrix water imbibition).

As mentioned in the introduction, for an accurate representation of temperature evolution, we had to consider heat loss through the bulkhead as well as out-of-plane heat loss in the rock mass. The heat-loss coefficient of 0.075 W/K-m^2 for heat loss through the bulkhead and 0.005 W/K-m^2 for out-of-plane heat loss into the rock resulted in a very good agreement between measured and simulated temperature (Fig. 1b) [5].

Table 1. Rock properties of the fractured welded tuff (Tptpmn unit) surrounding the DST experiment

Property	Value
Matrix Hydraulic and Thermal Properties	
Permeability	1.24E-17 m^2
Porosity	0.11
Van Genuchten, α_m	2.25E-6 Pa^{-1}
Van Genuchten m_m	0.247
Residual saturation	0.18
Rock grain density, ρ	2,530 kg/m3
Rock grain specific heat	953 J/kg K)
Dry thermal conductivity	1.67 W/m K
Wet thermal conductivity	2.0 W/m K
Fracture Hydrological and Hydro-Mechanical Properties	
Permeability, k	1.00E-13 m^2
Porosity	0.263E-3
Van Genuchten, α_f	9.73E-5 Pa^{-1}
Van Genuchten, m_f (-)	0.492
Residual saturation	0.01
Fracture frequency	4.32 m^{-1}
b_{max} for Equation (12)	37.6 μm
Exponent *d* for Equation (12)	0.07 MPa^{-1}
Rock Mass Mechanical Properties	
Young's Modulus	14.77 GPa
Poisson's ratio	0.21
Thermal Expan. Coeff.	$5+0.0583\times T\ 10^{-6}/°C$

Table 2. Initial conditions

Parameter	Approximate value at the level of DST[1]
Vertical stress, σ_{zi}	≈ 5.7 MPa
Min horizontal stress, σ_{yi}	≈ 2.9 MPa
Max horizontal stress, σ_{xi}	≈ 3.4 MPa
Initial temperature, T_i	≈ 25°C
Initial Fracture saturation	≈ 9%
Initial matrix saturation	≈ 90%
Initial gas pressure	≈ 0.9 bar

1) Approximate values of the depth-dependent parameters at the drift level.

4. RESULTS OF THM EVOLUTION DURING HEATING AND COOLING OF THE ROCK MASS

Fig. 4 and 5 present calculated contours of temperature, changes in stress normal to vertical fractures, changes in liquid fracture saturation, and the resulting permeability changes in the NW-striking fracture set at 4 years (end of heating) and 8 years (end of cooling). We present the results for the NW-striking subvertical fracture set because these are the permeability data used for comparison to the measured values.

Fig. 4a shows that at the end of the heating, the temperature has risen above the boiling point around the heated drift and near the wing heaters. High temperature induces strongly coupled TH processes with evaporation of liquid water and drying near the heat source (Fig. 4b, dryout zone). The evaporated water is transported as vapor away from the heat source toward cooler regions, where it is condensed to liquid water (Fig. 4b, dark zone). As a result, a dryout zone is created near the heat source and a condensation zone moves progressively away from the heat source. In the condensation zone, increases in fracture liquid saturation should result in a decrease in air permeability.

At the same time, high temperature gives rise to thermal expansion of the rock mass with associated thermal stresses (Fig. 4c). Near the heat source, the horizontal compressive stress increases strongly, with a maximum increase at the drift wall and near the wing heaters. Such an increase in compressive stress tends to tighten fractures to smaller aperture, leading to a reduction in air permeability. Away from the heat source, however, the horizontal stress decreases slightly. This reduction in horizontal stress will allow pre-existing vertical fractures to open to a larger aperture, leading to an increase in air permeability in this area.

Fig. 4d shows the calculated THM-induced changes in air permeability. These changes are caused by the combined effect of TH-induced changes in fracture moisture content (Fig. 4b) and TM-induced changes in fracture aperture (Fig. 4c). That is, the total permeability change factor caused by the combined effects of changes in TM- and TH-induced changes was calculated as:

$$F_k\left(\Delta\sigma_x, \Delta S_l\right) = F_k\left(\Delta\sigma_x\right) \cdot F_{krg}\left(\Delta S_l\right) \tag{13}$$

or

$$F_k^{THM} = F_k^{TM} \cdot F_k^{TH} \tag{14}$$

Fig. 4d shows that near the heat source, permeability decreases mainly because of fracture closure, but is also affected by TH-induced wetting and drying. Away from the heat source, about 20 m above the drift, a zone of slightly increased permeability has developed as a result of the opening of vertical fractures.

Fig. 5a shows that at the end of the cooling period, the temperature is still significantly elevated, with a temperature above 60°C near the drift and a zone of above 40°C extending to a distance of more than 30 m from the center of the drift.

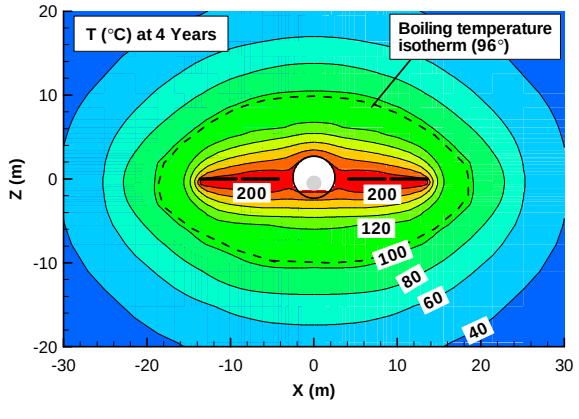

(a)

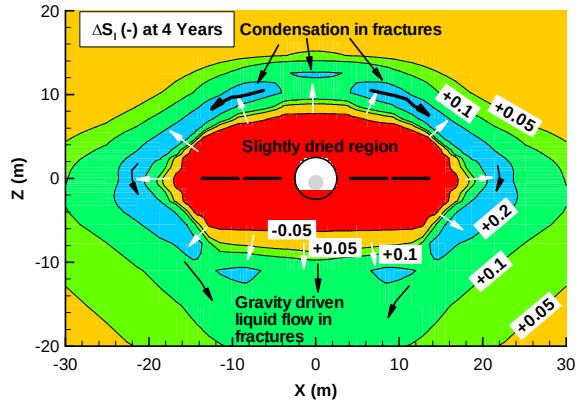

(b)

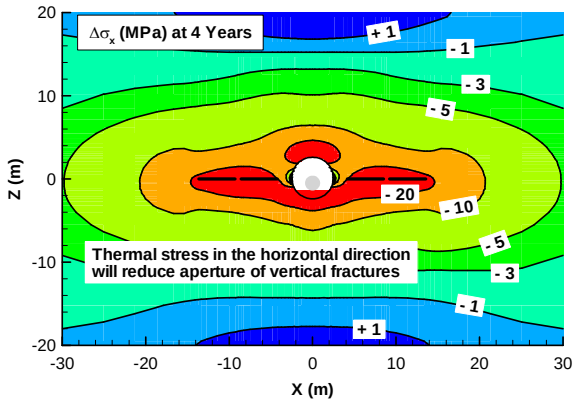

(c)

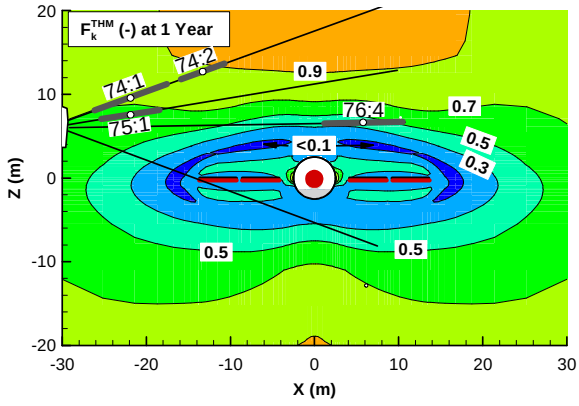

(d)

Fig. 4. Calculated contours of (a) temperature, (b) change in liquid fracture saturation, (c) change in horizontal stress, and (d) permeability change factor in the NW-striking fracture set after 4 years (at the end of the heating phase).

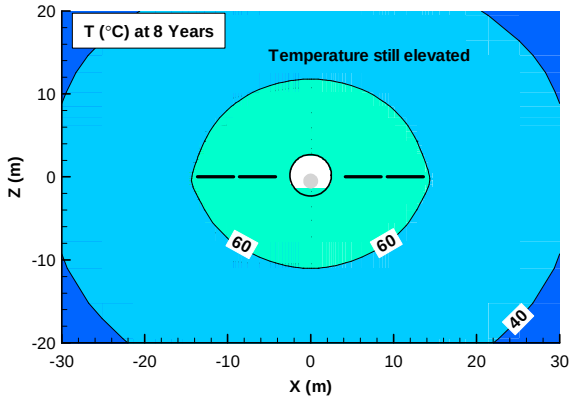

(a)

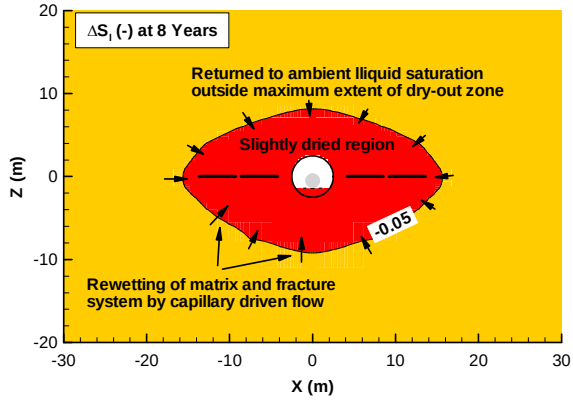

(b)

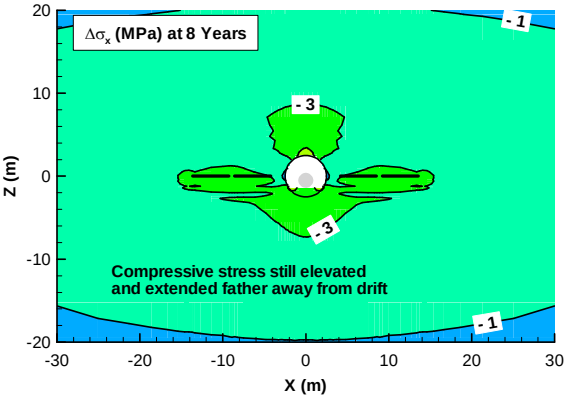

(c)

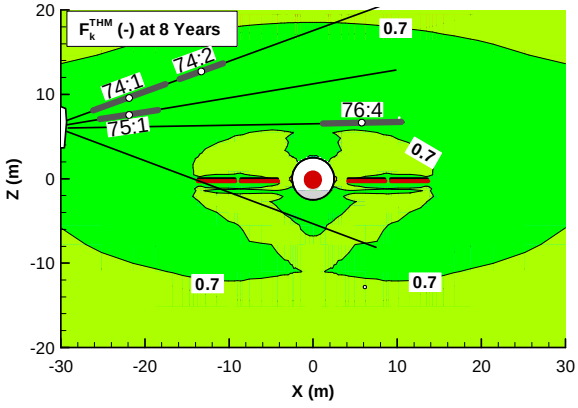

(d)

Fig. 5. Calculated contours of (a) temperature, (b) change in liquid fracture saturation, (c) change in horizontal stress, and (d) permeability change factor in the NW-striking fracture set after 8 years (at the end of the cooling phase).

The previously condensed water in the fracture system has either drained by gravity or been imbibed into the matrix (Fig. 5b). The dryout zone is rewetted by capillary suction, but in a zone around the Heated Drift and wing heaters the fracture system still remains slightly dryer than the initial preheating conditions.

The thermal stress has decreased with the decreasing temperature and with the loss of thermal gradient, but at the end of the cooling period, the horizontal compressive stress is still 1 to 3 MPa above its initial value (Fig. 5c). The resulting permeability change at the end of the cooling period is about 0.7 of its initial (pre-heating) value, and the permeability change is relatively uniformly distributed as a result of the uniform thermal stress (Fig. 5d). The calculated remaining permeability changes are entirely a result of the remaining thermal stress.

5. COMPARISON OF CALCULATED AND MEASURED AIR PERMEABILITY

Comparisons of measured and calculated evolution of air permeability for all 44 test intervals are presented in Rutqvist et al. [5]. In general, the numerical model could capture observed permeability changes very well during the heating phase. Specifically, the trends in the evolution of measured permeability (e.g., increases or decreases) were well captured by the model at most test intervals, although the measured data are scattered at several intervals, and there are systematic deviations between measured and calculated data at some intervals. The deviations between measured and calculated permeability values appeared to increase during the cooling period. In this paper, we present a few examples of comparison between calculated and measured data. All these examples are taken from the BH 74 to 78 borehole array (see Figs. 3, 4d and 5d).

5.1. Examples of Good Agreement Between Calculated and Measured Air Permeability

At several air-permeability test intervals located close to the heat source, the results indicate a significant signature of TH-induced change in permeability, in addition to the prominent TM-induced changes. For example, in interval 76:4, the permeability first decreases as a result of the superimposed effect of increasing stress and decreasing gas permeability (due to wetting), to reach a minimum of $k/k_i \approx 0.1$ at about 2 years (Fig. 6a). Thereafter, the modeling shows that some of the reduced permeability recovers as a result of drying of the previously wetted fractures and stabilizes at $k/k_i \approx 0.5$. The temporary wetting and subsequent drying is a result of the condensation zone shown in Fig. 4a, which progressively moves outward and successively crosses several air-injection intervals. The remaining $k/k_i \approx 0.5$, at about 4 years, is caused by the elevated horizontal stress that keeps the vertical fractures compressed to an aperture smaller than its initial value.

At some air-permeability test intervals, the model indicates that the observed changes in air permeability are caused entirely by stress-induced changes. These test intervals are located far above the Heated Drift, away from the maximum extent of the dryout and wetting zones. At such a distance from the heat source, the fractures stay dry, at the ambient liquid saturation of about 9%. For test intervals in these boreholes, we may compare calculated and measured TM-induced changes in permeability without interference for TH-induced changes. For example, in interval 75:1, the model shows that the permeability slowly decreases with increasing compressive horizontal stress, to reach a minimum of $k/k_i \approx 0.6$ at the end of the four-year heating period (Fig. 6b). Thereafter, as the rock mass cools down, the compressive stresses are reduced and the permeability recovers to reach a $k/k_i \approx 0.8$ at the end of the four-year cooling period. Thus, the remaining permeability reduction by a factor $k/k_i \approx 0.8$ is attributed to the remaining thermal stress keeping the fractures slightly compressed as the temperature is still elevated above ambient conditions.

5.2. Examples of Significant Difference Between Calculated and Measured Air Permeability

At several intervals, the measured response significantly deviates from that of the thermo-hydro-elastic solution, especially towards the end of the cooling period. For example, Fig. 7a presents one interval (74:1) at which a sudden increase in measured permeability occurred after about 5 to 6 years. Such sudden increase in permeability might be a result of shear reactivation and dilation along a fracture intersecting measurement interval 74:1. However, it is difficult to know whether this is the real cause of the observed permeability change, especially since corresponding increases were not noted in neighboring measurement intervals that would likely have been intersected by the same fracture. Note that the measured permeability change is moderate——just a factor of 1.8 higher than the original value.

In another example shown in Fig. 7b, the measured permeability was consistently lower than the calculated permeability and an irreversible permeability reduction was observed at the end of the cooling phase. Such permeability reduction (compared to the thermal-hydro-elastic solution) indicates irreversible contraction of the fracture surfaces, which may result from crushing or dissolution of highly stressed surface asperities under years of elevated stress and temperature conditions. Dissolution of surface asperities has been suggested as a mechanism that could explain field and laboratory observations of fracture-permeability decrease during increasing temperature, even under constant normal stress [14]. At this interval, the initial permeability was

relatively small, suggesting that the initial aperture could be small and that the pressure solution and associated mineral precipitation could be detectable even after a few years. However, the observed irreversible permeability decrease observed in some test intervals at the DST can only be considered as anecdotal evidence of such a process.

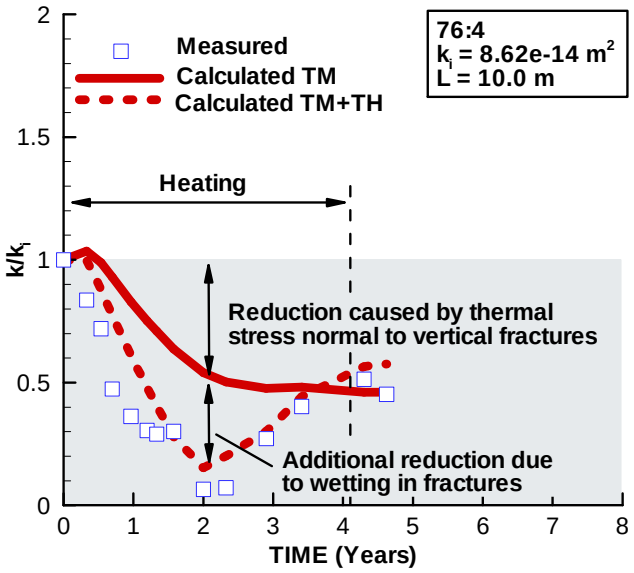

(a)

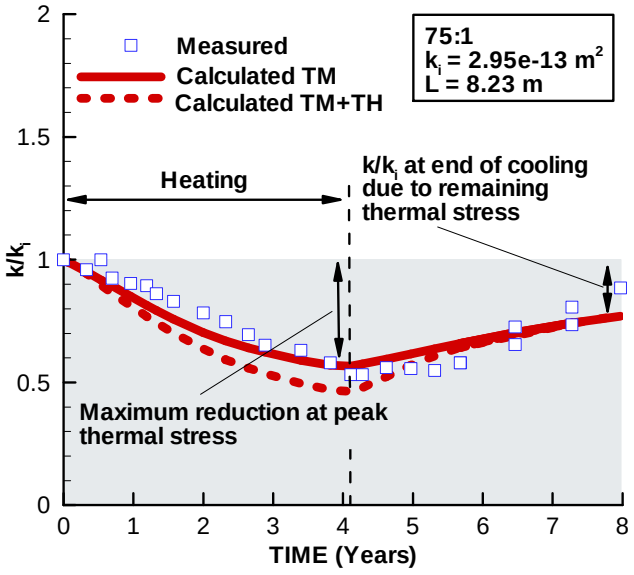

(b)

Fig. 6. Results from two test intervals in which a good agreement between calculated and measured responses were achieved and the stress- and moisture-induced changes can be clearly distinguished by the modeling: (a) Results at test interval 76:4, showing dependency of TM and TH responses; and (b) results at test interval 75:1, showing dependency on pure TM responses.

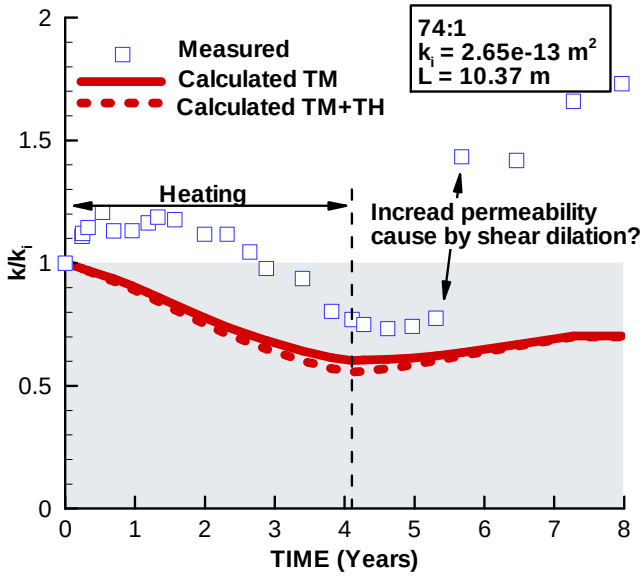

(a)

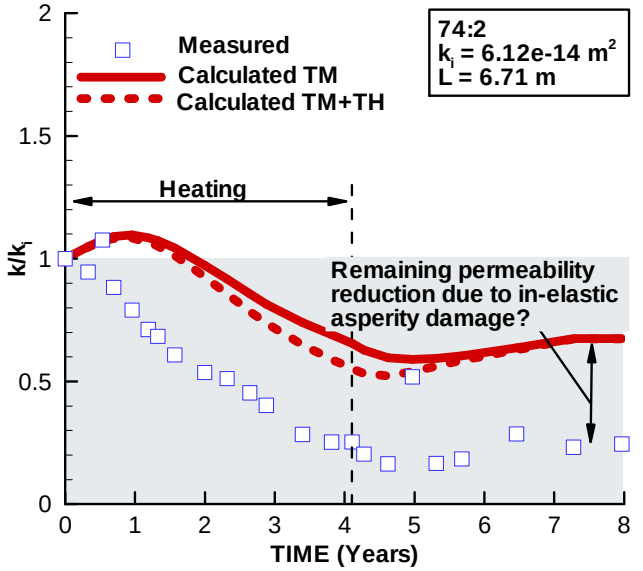

(b)

Fig 7. Results from two test intervals in which significant deviation between calculated and measured responses were observed and irreversible permeability changes are identified: (a) results at test interval 74:1, showing sudden increases in the measured permeability that might be attributed to fracture shear dilation; and (b) results at test interval 74:2, showing irreversible permeability decrease that might be attributed to fracture surface asperity shortening as a result of pressure solution.

6. CONCLUSIONS

We have conducted a coupled thermal, hydrological, and mechanical analysis of thermally induced permeability changes during heating and cooling of fractured volcanic rock at the Yucca Mountain Drift Scale Test, Nevada. The analysis extends a previous analysis of the four-year heating phase to include newly available data from the subsequent four-year cooling phase. The analysis of the entire eight-year experiment confirms our previous results, showing that the observed changes in air permeability at the site can be explained by a combination of thermal-mechanically-induced changes in fracture aperture and moisture-induced changes (Fig. 8). However, the analysis of the new cooling phase data also indicates irreversible permeability changes that significantly deviated from the reversible thermo-hydro-elastic solution. The identified irreversible permeability changes may be attributed to inelastic thermal-mechanical processes consistent with either inelastic fracture shear dilation (where permeability increased) or inelastic fracture surface asperity shortening (where permeability decreased). The observed permeability changes remaining at the end of the cooling phase ranged from 0.2 to 1.8 of the original (pre-heating) permeability.

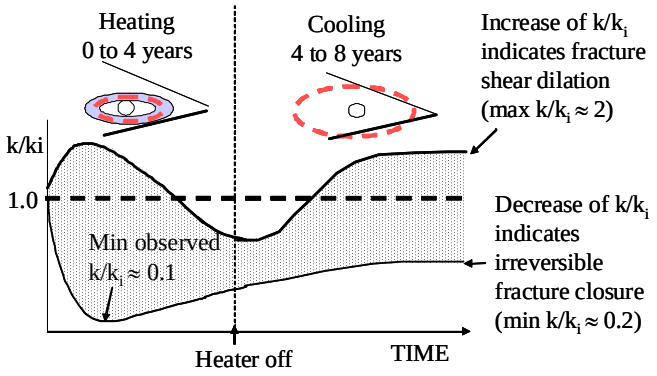

Fig. 8. Overall observed permeability responses at the Drift Scale Test and interpretation of their causes based on the coupled THM analysis.

ACKNOWLEDGMENTS

We are grateful for reviews by Dr. Hui-Hai Liu and Dr. Dan Hawkes of Lawrence Berkeley National Laboratory, which substantially improved this paper. The work was supported by the Office of Civilian Radioactive Waste Management, Office of the Chief Scientist, of the U.S. Department of Energy under Contract No. DE-AC02-05CH11231.

REFERENCES

1. Wagner, R. 2002. Thermal Testing Measurements Report. TDR-MGR-HS-000002 REV00 ICN 00. Las Vegas, Nevada: Bechtel SAIC Company.

2. Rutqvist, J., D. Barr, R. Datta A. Gens, M. Millard, S. Olivella, C.-F. Tsang, and Y. Tsang. 2005. Coupled thermal-hydrological-mechanical analysis of the Yucca Mountain Drift Scale Test – comparison of field results to predictions of four different models. *In.t J. Rock Mech Min. Sc.* 42:680–697.

3. Hsiung, S.M., A.H. Chowdhury, and M.S. Nataraja. 2005. Numerical simulation of thermal-mechanical processes observed at the drift-scale heater test at Yucca Mountain, Nevada, USA. *In.t J. Rock Mech Min. Sc.* 42:652–666.

4. Olivella, S., and A. Gens. 2005. Double structure THM analyses of a heating test in a fractured tuff incorporating intrinsic permeability variations. *In.t J. Rock Mech Min. Sc.* 42:667–679.

5. Rutqvist, J., B. Freifeld, Y.S., K.-B. Min, D. Elsworth, and Y. Tsang. 2008. Analysis of Thermally Induced Changes in Fractured Rock Permeability during Eight Years of Heating and Cooling at the Yucca Mountain Drift Scale Test. In.t J. Rock Mech Min. Sc. (Accepted).

6. Rutqvist, J., Y.S. Wu, C.-F. Tsang, and G.A. Bodvarsson. 2002. Modeling Approach for Analysis of Coupled Multiphase Fluid Flow, Heat Transfer, and Deformation in Fractured Porous . *In.t J. Rock Mech Min. Sc.* 39:429–442.

7. Tsang, Y.W., and J.T. Birkholzer. 1999. Predictions and Observations of the Thermal-Hydrological Conditions in the Single Heater Test. *J. Cont. Hydrol.* 38: 385–425.

8. Birkholzer, J.T., and Y.W. Tsang. 2000. Modeling of thermal-hydrologic processes in a large-scale underground heater test in partially saturated tuff. *Water Resourc. Res.* 36: 1431–1447.

9. Hinds, J.J., G.S. Bodvarsson, and G.H. Nieder-Westermann. 2003. *J. Cont. Hydrol.* 62–63:111–132.

10. Wang, J., P. Cook, R. Trautz, S. Flexser, Q. Hu, R. Salve, D. Hudson, M. Conrad, Y. Tsang, K. Williams, W. Sol, and J. Turin. 2001. In-situ field testing of processes ANL-NBS-HS-000005 REV01. Las Vegas, Nevada: Bechtel SAIC Company.

11. Witherspoon, P.A., J.S.Y. Wang, K. Iwai, and J.E. 1980. Validity of cubic law for fluid flow in a deformable rock fracture. *Water. Resourc. Res.* 16:1016-1024.

12. Leverett, M.C. 1941. Capillary behavior in porous media. *Trans. AIME.* 142: 341–358.

13. van Genuchten, MT. 1980. A closed-form equation for predicting the hydraulic conductivity of unsaturated soils. *Soil. Sci. Soc. Am. J.* ;44:892–898.

14. Min KB, Rutqvist J, Elsworth D. Chemically- and mechanically-mediated influences on the transport and mechanical characteristics of rock fractures. Submitted for publication. 30 pp.